Proceedings of IMECE'03
2003 ASME International Mechanical Engineering Congress
Washington, D.C., November 15–21, 2003

IMECE2003-41552

VIBRATION AND SOUND RADIATION OF SANDWICH BEAMS WITH HONEYCOMB TRUSS CORE

M. Ruzzene
School of Aerospace Engineering
Georgia Institute of Technology
Atlanta, GA 30332–0150

ABSTRACT

The vibrations of and the sound radiation from sandwich beams with truss core are here analyzed. The structure of the core is composed of a sequence of identical unit cells repeating along the beam length and across the core thickness. Each cell is composed of beam elements assembled to form a frame structure. Layouts with honeycomb patterns arranged through the thickness of the core are considered. This design represents an alternative with respect to the traditional application of honeycombs in sandwich construction. The proposed configuration provides sandwich beams with interesting structural as well as acoustic characteristics. A spectral finite element model is developed to evaluate the structural and the acoustic behavior of the considered class of sandwich beams. The spectral model can be easily coupled with a Fourier Transform based analysis of the sound radiated by the fluid-loaded structure. The model predicts the performance of beams with various core configurations. The comparison is carried out in terms of vibration and sound radiation in an unbounded acoustic half-plane. Hexagonal and re-entrant honeycomb configurations are considered to study the effects of core geometry on structural response and acoustic radiation.

INTRODUCTION

The multifunctional properties of cellular solids have generated great interest for their application in ultra-light structures. The properties that appear most attractive are those that govern the use of cellular solids as cores for panels and shells having lower weight than competing materials, and potentially superior heat dissipation, vibration control and energy dissipation characteristics [1-3]. Commercially available cellular solids and foams have random microstructures and their properties have been thoroughly documented (see for example [1,3]). An interesting research trend in cellular materials consists in the study and the application of deterministic periodic architectures, whose topology can be designed and tailored for the considered component to achieve performances greatly superior than those demonstrated by their stochastic analogues [3]. The scalable geometry of deterministic periodic architectures, whereby the structural properties depend on the actual size of the unit cells, allows for their application to both small-scale and large-scale structural systems. Examples of applications of deterministic periodic cellular architectures include the lattice material and prismatic core concepts [2,5]. Both configurations have been employed and studied in the past as alternative core configurations for sandwich structures with superior structural characteristics and potential multifunctional capabilities. For example, the application of the lattice material concept has lead to the design of truss core sandwich constructions, whose optimized structural performance has proven to be competitive with traditional sandwich honeycomb and stiffened structures [5].

In this paper, the dynamic response and the sound radiation of truss core sandwich beams is investigated. The structural-acoustic performance of periodic truss core panels has been investigated by El-Raheb, who in [6] studied the frequency response of two-dimensional panels using the transfer matrix method, and in [7] presented an interesting hybrid technique to predict their elasto-acoustic behavior. In his work, El-Raheb focused on the analysis of the performance of panels with a given configuration and evaluated the effect on the response of a number of parameters, such as fluid-loading and damping. This paper analyzes the performance of sandwich beams with truss core elements arranged according to a honeycomb configuration. In the proposed design, the honeycomb topology is developed across the thickness of the sandwich structure, as opposed to the layout of conventional honeycomb sandwich constructions. The proposed sandwich beams hence can be more appropriately described as examples of applications of prismatic materials as defined in [2], and the "truss core" terminology used throughout the paper should be considered as having a wider meaning. The proposed honeycomb configurations are an alternative to the truss-like panels presented in [6,7]. The core results from the assembly of unit

cells, whose shape and geometry are defined by the cell aspect ratio and by an internal angle. Focus is placed in the analysis of the performance of cores with re-entrant geometries as described in [1,8]. Re-entrant cellular architectures have been widely studied in the past as viable alternatives for the design of honeycomb cores with superior shear modulus and compressive strength [9,10]. Re-entrant two-dimensional cellular structures have also shown unique beaming characteristics, whereby the propagation of elastic waves at given frequencies is restricted to specified directions [11].

The dynamic behavior of the considered sandwich beams is predicted by a finite element model, which employs shape functions derived directly from the solution of distributed parameter models for each beam element. This formulation, often denoted as "spectral" [12-14], accurately describes the dynamic response of the structure with a reduced number of elements. The considered dynamic shape functions are in fact able to capture the response of each element for given nodal displacements, even for high excitation frequencies. The developed model also allows capturing local phenomena, such as for example the resonance of each core element, that help understanding the fundamentals of operation of the considered structures and provide important guidelines for their optimal design. In addition, the spectral formulation can be easily and efficiently coupled with the Fourier Transform (FT) based analysis of the structure's sound radiation in a surrounding acoustic medium. Hence the proposed formulation is an efficient numerical tool for the analysis of the dynamic and acoustic performance of the considered truss core sandwich beams.

CONCEPT AND CONFIGURATION

The considered sandwich beam features a truss-type core with elements arranged according to a honeycomb configuration. The honeycomb geometry is laid out across the thickness of the core, as depicted in Figure 1. The core is obtained by the assembly of identical cells, which are replicated along the length of the beam and across the thickness of the core. Examples of the considered unit cell topologies are shown in Figures 2. The cell geometry is defined by its dimensions L_x and L_y and by the internal angle θ. For example, an internal angle θ =30^o and a cell aspect ratio $L_x / L_y = \sqrt{3}$ define a regular hexagonal honeycomb configuration. Several configurations for the core can be obtained by modifying the aspect ratio or the internal angle. For assigned beam length and core thickness, the aspect ratio determines the number of cells across the thickness and along the length of the beam, while the internal angle defines the cell shape. The beams depicted in Figures 2 both have a core composed of 2 cells across the thickness and 10 cells along the beam length. The performance of cores defined by positive (counterclockwise) (Figure 2.a) and negative (clockwise) internal angles (Figure 2.b) are here considered. The vibro-acoustic behavior of this class of sandwich beams is compared with that of truss core beams of the kind studied in [6,7] and schematically depicted in Figure 3. In this paper, the core depicted in Figure 3 will be denoted as "square", as opposed to the honeycomb cores shown in Figure 2.

In the considered configuration (Figure 4), the beam is part of a rigid baffle of infinite length. The bottom layer is excited by a plane incident pressure wave varying harmonically in time, while the top layer faces an unbounded half-plane fluid domain. The vibration of the bottom layer induced by the incident pressure wave is transmitted through the core to the top layer, which as a result radiates sound in the fluid domain.

VIBRATION OF BEAMS WITH TRUSS CORE: SPECTRAL FINITE ELEMENT MODELING

The considered sandwich beam is modeled as a frame structure [15], where core elements are oriented in the *xy* plane according to assigned topologies (Figure 2). The dynamic behavior of each element is described in the local reference system $\xi\psi$, rotated with respect to the global reference system *xy* of the angle φ (Figure 5).

Distributed parameter model in the local reference system

Each element is considered as an Euler-Bernoulli beam. Accordingly, in the local reference system, the beam's strain and kinetic energies are given by:

$$U = \frac{1}{2} EA \int_0^L u_\xi^2(\xi,t)d\xi + \frac{1}{2} EI \int_0^L w_{\xi\xi}^2(\xi,t)d\xi \qquad (1)$$

$$T = \frac{1}{2} m \int_0^L \dot{u}_t^2(\xi,t) + \dot{w}_t^2(\xi,t)d\xi \qquad (2)$$

where E is the Young's Modulus of the beam material, A, I are respectively the area and the second moment of area of the beam cross section, and m is the mass per unit length of the beam. Subscripts ξ and t in equations (1) and (2) respectively denote partial differentiation with respect to the longitudinal coordinate ξ and time t. Also, in equations (1) and (2) u and w are the axial and the transverse displacement of the beam in the local coordinates.

The work of the external forces can be expressed as:

$$W = \int_0^L u(\xi,t)\cdot q_u(\xi,t)d\xi + \int_0^L w(\xi,t)\cdot q_w(\xi,t)d\xi \qquad (3)$$

where $q_u(\xi,t), q_w(\xi,t)$ are externally applied distributed longitudinal and transverse loads per unit length.

The following set of partial differential equations describe the beam's longitudinal and transverse harmonic motion at frequency ω.

$$\begin{aligned} K\cdot u_{\xi\xi}(\xi,\omega) + \omega^2\cdot m\cdot u(\xi,\omega) &= -q_u(\xi,\omega) \\ D\cdot w_{\xi\xi\xi\xi}(\xi,\omega) - \omega^2\cdot m\cdot w(\xi,,\omega) &= -q_w(\xi,\omega) \end{aligned} \qquad (4)$$

where $K=EA$ and $D=EI$ are the beam's longitudinal and flexural rigidities.

Degrees of freedom and shape functions

The homogeneous solution for equations (4) can be found in the form:

$$u(\xi,\omega) = a_1 \cdot e^{k_a \cdot \xi} + a_2 \cdot e^{-k_a \cdot \xi}$$
$$w(\xi,\omega) = a_3 \cdot e^{k_{b1} \cdot \xi} + a_4 \cdot e^{-k_{b1} \cdot \xi} + a_5 \cdot e^{k_{b2} \cdot \xi} + a_6 \cdot e^{-k_{b2} \cdot \xi} \quad (5)$$

where a_i (i=1,..,6) are integration constants, and where:

$$k_a = (\omega^2 \frac{m}{K})^{1/2},\ k_{b1} = (\omega^2 \frac{m}{D})^{1/4};\ k_{b2} = i(\omega^2 \frac{m}{D})^{1/4} \quad (6)$$

are the wavenumbers of the longitudinal and transverse elastic waves. Equation (5) can be also expressed in matrix form as follows:

$$\begin{Bmatrix} u(\xi,\omega) \\ w(\xi,\omega) \end{Bmatrix} = [H(\xi,\omega)] \cdot \{a\} \quad (7)$$

The vector of the integration constants $\{a\}$ can be expressed in terms of the displacements and cross-section rotation of the two ends of the beam:

$$\{a\} = [T(\omega)]^{-1} \cdot \left\{\delta^{(e)}(\omega)\right\} \quad (8)$$

where $[T(\omega)]$ is a transformation matrix obtained by imposing the displacement at the element boundaries, and $\left\{\delta^{(e)}\right\}$ is the vector of the element nodal displacements defined as:

$$\left\{\delta^{(e)}\right\} = \left\{ u_i \quad w_i \quad w_{\xi_i} \quad u_f \quad w_f \quad w_{\xi_f} \right\}^T \quad (9)$$

where i and f denote the initial and final node of the considered beam element (see Figure 5), and where $w_\xi = \partial w / \partial \xi$ is the slope of the cross section at the considered location.

Substituting equation (8) into equation (7) yields:

$$\begin{Bmatrix} u(\xi,\omega) \\ w(\xi,\omega) \end{Bmatrix} = [N(\xi,\omega)] \cdot \left\{\delta^{(e)}(\omega)\right\} \quad (10)$$

where $[N(\xi,\omega)]$ is the matrix of shape functions. The shape functions are obtained from the solution of the beam's distributed parameter model for harmonic motion at frequency ω. Within the validity of Euler-Bernoulli assumptions, these shape functions reproduce the exact displacement of the considered beam element for the assigned set of nodal displacements. Accordingly a single finite element is sufficient to fully characterize the response of the beam for any value of frequency ω. This finite element formulation, often denoted as "spectral" [12-14], allows an accurate prediction of the dynamic response of the global structure by using a reduced number of elements. As opposed to traditional finite element formulations, the number of elements does not need to be increased to fully capture the dynamic response at high frequencies. Finally, the spectral formulation can be easily modified to include the effects of the interaction of the vibrating structure with a surrounding fluid medium. Particularly, the spectral model nicely ties with a FT-based analysis of the beam sound radiation in the surrounding acoustic domain.

Spectral mass and stiffness matrices and load vector.

Substituting equation (10) in the expressions of the strain and kinetic energy for the considered beam element gives:

$$U^{(e)}(\omega) = \frac{1}{2} \cdot \left\{\delta^{(e)}(\omega)\right\}^T \left[K^{(e)}(\omega)\right] \left\{\delta^{(e)}(\omega)\right\} \quad (11)$$

$$T^{(e)}(\omega) = -\frac{\omega^2}{2} \cdot \left\{\delta^{(e)}(\omega)\right\}^T \left[M^{(e)}(\omega)\right] \left\{\delta^{(e)}(\omega)\right\} \quad (12)$$

where $\left[K^{(e)}(\omega)\right]$ and $\left[M^{(e)}(\omega)\right]$ are respectively the beam stiffness and mass spectral matrices for element *(e)*, obtained in the local reference system and at the given frequency ω.

Similarly the work of the external loads W can be expressed as:

$$W^{(e)}(\omega) = \left\{f^{(e)}(\omega)\right\}^T \left\{\delta^{(e)}(\omega)\right\} \quad (13)$$

where $\left\{f^{(e)}(\omega)\right\}$ is the load vector.

Equation of motion in the global reference system

The components of the beam longitudinal and transverse displacements u,w with respect to the global reference system xy are given by:

$$u = U \cdot \cos\varphi + W \cdot \sin\varphi$$
$$w = -U \cdot \sin\varphi + W \cdot \cos\varphi \quad (14)$$

where φ is the rotation angle of the local axis ξ with respect to the global axis x (see Figure 5), and U, W are the displacement components along x and y. Accordingly the vector of nodal displacements in the global reference system $\left\{\Delta^{(e)}(\omega)\right\}$ is related to the local nodal displacements vector $\left\{\delta^{(e)}(\omega)\right\}$ through a rotation matrix $[R]$:

$$\left\{\delta^{(e)}(\omega)\right\} = [R] \cdot \left\{\Delta^{(e)}(\omega)\right\} \quad (15)$$

Substituting equation (15) in the expression of the strain and kinetic energy gives:

$$U^{(e)}(\omega) = \frac{1}{2} \cdot \left\{\Delta^{(e)}(\omega)\right\}^T \left[K_r{}^{(e)}(\omega)\right] \left\{\Delta^{(e)}(\omega)\right\} \quad (16)$$

$$T^{(e)}(\omega) = -\frac{\omega^2}{2} \cdot \left\{\Delta^{(e)}(\omega)\right\}^T \left[M_r{}^{(e)}(\omega)\right] \left\{\Delta^{(e)}(\omega)\right\} \quad (17)$$

where $\left[K_r{}^{(e)}(\omega)\right]$ and $\left[M_r{}^{(e)}(\omega)\right]$ are the rotated, as denoted by subscript '*r*', mass and stiffness spectral matrices in the xy reference system.

Similarly, the work of the external forces can be rewritten as:

$$W^{(e)}(\omega) = \left\{F^{(e)}(\omega)\right\}^T \left\{\Delta^{(e)}(\omega)\right\} \quad (18)$$

where $\left\{F_r{}^{(e)}(\omega)\right\} = [R]^T \cdot \left\{f^{(e)}(\omega)\right\}$ is the load vector in the global reference system.

The spectral formulation described above considers the dynamic problem associated with the beam's vibration at frequency ω, as a static equilibrium problem [12, 13]. A spectral energy functional can be defined for element *(e)* as:

$$\Pi^{(e)}(\omega) = U^{(e)}(\omega) + T^{(e)}(\omega) - W^{(e)}(\omega) \tag{19}$$

The spectral energy functional for the whole sandwich beam structure is given by:

$$\begin{aligned} &\Pi(\omega) = U(\omega) + T(\omega) - W(\omega) \\ &\Pi(\omega) = \frac{1}{2}\{\Delta(\omega)\}^T \left([K(\omega)] - \omega^2[M(\omega)]\right)\{\Delta^{(e)}(\omega)\} \\ &\quad - \{F(\omega)\}^T\{\Delta^{(e)}(\omega)\} \end{aligned} \tag{20}$$

where $[K(\omega)], [M(\omega)], \{F(\omega)\}$ are the structure's mass and stiffness matrices and global load vector, obtained from the element matrices and vector through standard finite element assembly procedures.

Applying the Theorem of Minimum Total Potential [16] yields the following spectral equation of motion for the sandwich beam:

$$\left([K(\omega)] - \omega^2[M(\omega)]\right)\{\Delta^{(e)}(\omega)\} = \{F(\omega)\} \tag{21}$$

Solution of equation (21) for an assigned frequency ω gives the amplitude of the displacements at each node. The displacements within each element can be then obtained through the shape functions as described by equation (10).

SOUND RADIATION IN THE ACOUSTIC DOMAIN

The considered configuration for the sandwich beam is depicted in Figure 4. The bottom layer is excited by a plane pressure incident wave, which varies harmonically in time and can be expressed as:

$$p_i(x,y,t) = p_i(x,y,\omega)e^{-i\omega t} \tag{22}$$

where

$$\begin{aligned} p_i(x,y,\omega) &= p_{io} \cdot e^{ik_x x + ik_y y} \\ &= p_{io} \cdot e^{ik(x\sin\alpha + y\cos\alpha)} \end{aligned} \tag{23}$$

In equation (23), p_{io} is the amplitude of the incident pressure, α is the angle of incidence measured with respect to the y axis, and $k = \omega / c_a$ is the acoustic wave number, with c_a denoting the speed of sound in air.

According to Figure 4, the top layer of the beam interacts with and radiates into an unbounded fluid domain. The equation of motion and the spectral formulation for the elements of the top layer are modified to include the effect of their interaction with the fluid. Also, the spectral formulation is coupled with a FT-based analysis of the pressure radiated in the fluid domain [17,18].

Spectral load vector equivalent to the incident pressure

Each element belonging to the bottom layer is loaded by an incident pressure wave expressed by equation (28). The work of the distributed load corresponding to the incident pressure at frequency ω is given by

$$W^{(e)}(\omega) = \int_0^{L^{(e)}} w(\xi,t) \cdot p_i(\xi, y_b, \omega) \cdot b \cdot d\xi \tag{24}$$

where y_b defines the location of the elements of the bottom layer in the global reference system, b is the beam off-plane width, $L^{(e)}$ is the element length, w is the element's transverse displacement. The local longitudinal coordinate ξ for the bottom layer elements is aligned with the global x axis (See Figure 5).

Imposing the shape functions, as defined in equation (10), gives:

$$\begin{aligned} W^{(e)}(\omega) &= \int_0^{L^{(e)}} \left(p_i(x,0,\omega) \cdot [N(\xi,\omega)] \cdot b \cdot d\xi\right) \cdot \{\delta^{(e)}(\omega)\} \\ &= \{f^{(e)}(\omega)\}^T \{\delta^{(e)}(\omega)\} \end{aligned} \tag{25}$$

where $\{f^{(e)}(\omega)\}$ is the spectral element load vector equivalent to the applied pressure distribution.

Sound radiation in the fluid domain: Fourier Transform solution

The pressure distribution in the acoustic fluid domain facing the top layer of the beam can be obtained from the solution of Helmholtz equation [17]:

$$\left(\frac{\partial^2}{\partial x^2} + \frac{\partial^2}{\partial y^2} - k^2\right) p_t(x,y,\omega) = 0 \tag{26}$$

with the following boundary conditions:

$$\left.\frac{\partial p_t(x,y,\omega)}{\partial y}\right|_{y=0} = \rho_f \omega^2 w_t(x,\omega) \tag{27}$$

where ρ_f is the density of the fluid, $p_t(x,y,\omega)$ is the pressure radiated in the fluid, and $w_t(x,\omega)$ is the transverse displacement of the top layer (Figure 6).

A solution for equation (26) can be conveniently found by considering the FT of Helmholtz equation with respect to the coordinate x, which gives [17]:

$$\left(\frac{\partial^2}{\partial y^2} + \gamma_x^2 - k^2\right) \hat{p}_t(\gamma_x, y, \omega) = 0 \tag{28}$$

The FT of the pressure $\hat{p}_t(\gamma_x, y, \omega)$ must satisfy the transformed boundary conditions:

$$\left.\frac{\partial \hat{p}_t(\gamma_x, y, \omega)}{\partial y}\right|_{y=0} = \rho_f \omega^2 \hat{w}_t(\gamma_x, \omega) \tag{29}$$

where $\hat{w}_t(\gamma_x, \omega)$ is the FT of the beam's transverse displacement given by:

$$\hat{w}_t(\gamma_x,\omega)=\int_{-L/2}^{L/2} w_t(x,\omega)\cdot e^{-i\cdot\gamma_x x}dx \qquad (30)$$

In equation (30), the integration is limited to the length of the beam L, as the baffle is considered to be infinitely rigid and not undergoing any transverse motion (see Figure 6).

The solution of equation (28) with boundary conditions expressed by equation (29) is given by:

$$\hat{p}_t(\gamma_x,y,\omega)=-i\cdot\rho_f\cdot\omega^2\cdot\hat{w}_t(\gamma_x,\omega)\cdot\frac{e^{i\cdot y\cdot\sqrt{k^2-\gamma_x^2}}}{\sqrt{k^2-\gamma_x^2}} \qquad (31)$$

The pressure distribution in the fluid domain is then obtained through the Inverse Fourier Transform:

$$p_t(x,y,\omega)=\frac{1}{2\pi}\int_{-\infty}^{+\infty}\hat{p}_t(\gamma_x,y,\omega)\cdot e^{i\cdot\gamma_x x}d\gamma_x \qquad (32)$$

Evaluation of transform solution through the spectral formulation

The spectral formulation presented in above allows an easy application and numerical implementation of the Fourier Transform solution for the radiated pressure. Discretizing the structure into finite elements and using dynamic shape functions such as those defined in equation (10) makes the evaluation of the displacement transform particularly simple. The integral over the finite length of the beam in equation (30) can be in fact evaluated as the sum of integrals over each element of the top layer, which can be expressed as:

$$\hat{w}_t(\gamma_x,\omega)=\sum_{k=1}^{N_t}\int_0^{L^{(k)}} w_t(\xi,\omega)\cdot e^{-i\cdot\gamma_x(\xi-L^{(k)}/2)}d\xi \qquad (33)$$

where N_t is the number of elements belonging to the top layer and where $L^{(k)}$ is the length of the k-th element. Imposing the shape functions defined in equation (10) gives an expression for the displacement transform in terms of the vector of element nodal degrees of freedom $\{\delta^{(k)}\}$:

$$\hat{w}_t(\gamma_x,\omega)=\sum_{k=1}^{N_t}\int_0^{L^{(k)}}[N(\xi,\omega)]\cdot e^{-i\cdot\gamma_x(\xi-L^{(k)}/2)}d\xi\cdot\{\delta^{(k)}\} \qquad (34)$$

The exponential form of the considered shape functions allows the analytical evaluation of the integrals in equation (34), which results in the exact evaluation of the displacement transform for given γ_x and frequency ω. The pressure distribution can be then determined through the numerical estimation of the inverse pressure transform. The analytical estimation of the displacement coefficients in equation (34) reduces the approximation introduced by the numerical evaluation of the pressure distribution.

PERFORMANCE OF BEAMS WITH HONEYCOMB TRUSS CORE

Overview

The spectral formulation and the analysis of the sound radiation in the unbounded fluid medium are applied to evaluate the vibro-acoustic performance of beams with honeycomb truss core. Several configurations for the core are considered to estimate the effect of the core geometry and configuration on the performance of the beam. The various configurations can be obtained by varying the cell aspect ratio and internal angle. Focus is here placed in the evaluation of the influence of the internal angle on the beam's performance. Simulations are performed for θ varying between -45° and 30° for cores composed of 10 cells along the beam length and 1 cell across the thickness. The influence of varying numbers of cells in the core will be addressed in future papers.

The performance of beams with honeycomb truss core is compared to that of the beams with square core structure studied in [6,7] and shown in Figure 3. The analysis is carried out in terms of dynamic response, vibration and sound transmission loss indexes, and pressure radiated in the fluid domain. The goal of the study is the assessment of the effectiveness of the considered class of sandwich structures as acoustic panels and for vibration isolation applications.

Geometry and material properties

The beams are 1 m long and have a 4 cm thick core. Both layer and core elements are made of aluminum (Young's modulus 7.1E10 Pa, density 2700 kg/m^3), and have rectangular cross sections. The same material is considered for the constraining layers and the core, which is a common configuration for prismatic beams [4-6]. The top and bottom layers are 5 mm thick, while the thickness of the elements of the core is 2.5 mm. The out-of-plane width of the structure b is constant for every element and set equal to unity for simplicity. Damping is introduced by considering a complex modulus for all the elements ($E=E^*(1+i\eta)$), with a loss factor η=0.01. In all the simulations the beams are connected to the rigid baffle by pin joints, thus simulating simply supported boundary conditions.

The fluid in contact with the top layer is air (ρ_f= 1.2 kg/m^3, c_a=343 m/s). The beams are excited by plane pressure waves described by equation (23) incident on the bottom layer according to the configuration depicted in Figure 4. Normally incident waves (α=0) of unit amplitude (p_{io}=1 Pa) and frequency ω varying between 0 and 2000 Hz are here considered. The beams' performance for oblique incidence will be considered in future studies, to evaluate additional effects, such as coincidence, and the contribution of additional modes other than the odd ones on sound radiation.

Structural response and Vibration Transmission Loss

The spectral formulation presented above is used to predict the dynamic response of the considered class of sandwich beams. Examples of the results are shown in Figures 7.a and 7.b, where the response at mid-span of the top and bottom layers of beams with different core configurations are plotted

and compared. The beam with square core is used as a baseline. An initial analysis of the plots indicates that in the considered frequency range, a higher modal density characterizes the beams with honeycomb core. The square core beam has a higher stiffness than the beams with honeycomb core, as indicated by the lower amplitude of the displacement at zero frequency. The first resonance frequency of beams with honeycomb core is also lower. Static stiffness and resonance frequencies are affected by the core geometry, the re-entrant configurations being generally more compliant statically and having lower first resonance frequencies. The responses for the top and bottom layer look very similar, indicating that there is little vibration reduction through the core of the beam. A close analysis of the plots however indicates that the core becomes more effective in reducing the transmission of vibrations at frequencies closer to the upper limit of the considered range.

The effectiveness of the considered configuration in terms of vibration isolation capabilities can be evaluated through a vibration transmission coefficient τ_v, defined as the ratio of the average deflection kinetic energy of the top layer to that of the bottom layer. This definition is similar to the acoustic transmission coefficient [18] and for harmonic motion at frequency ω it can be expressed as:

$$\tau_v = \frac{\int_0^L \omega^2 \cdot w_t(x,\omega) \cdot w_t^*(x,\omega) \cdot dx}{\int_0^L \omega^2 \cdot w_b(x,\omega) \cdot w_b^*(x,\omega) \cdot dx} \qquad (35)$$

where w_b and w_l respectively denote the transverse deflection of the bottom and top layers and where the subscript (*) denotes a complex conjugate. In equation (35), it is assumed that the two layers have the same density and cross section properties.

The Vibration Transmission Loss (*VTL*) index can be defined in terms of the vibration transmission coefficient τ_v as follows:

$$VTL = 10 log_{10}(\frac{1}{\tau_v}) \qquad (36)$$

The *VTL*s for beams with the considered core configurations are shown and compared in Figure 8. The plots confirm the conclusions anticipated by the analysis of Figures 7, by clearly demonstrating that at low frequencies (<200 Hz), none of the considered core configurations is effective in reducing the transmission of vibrations. A significant difference in effectiveness can be however observed for frequencies above 200 Hz, where honeycomb cores generally perform better than the square core type beam. The performance of re-entrant geometries is particularly promising, especially for higher negative values of the internal angle (θ=-45^o).

The beams' deformed configurations for excitations at 200, 800 and 1500 Hz are shown in Figures 9 through 11. The frequencies are selected as representative of the beams' performance over the considered frequency range (0-2000 Hz). These deformed configurations are obtained by applying the dynamic shape functions (equation (10)) to interpolate the displacements within each element. The plots indicate that the higher the excitation frequency the higher the deformation of the core elements. Particularly noticeable at 800 and 1500 Hz are the sagging deformations of the horizontal members in the core with θ=-45^o (Figure 11), which, according to Figure 8, is the most efficient configuration in isolating the top and bottom layers. These results suggest that the vibration isolation characteristics can be enhanced by designing truss cores which undergo significant deformations, possibly caused by their local resonance (see also [6]), in a desired frequency range. The application of such design guidelines will be further investigated and addressed in future studies.

Sound radiation and Sound Transmission Loss

The acoustic performance of the considered class of beam structures and their potential application for sound transmission reduction is investigated through the evaluation of the Sound Transmission Loss (*STL*) index and by evaluating the sound radiation in the acoustic domain interacting with the top layer of the beam.

The Sound Transmission Loss (*STL*) is defined as:

$$STL = 10 log_{10}(\frac{1}{\tau_s}) \qquad (37)$$

where the sound transmission coefficient τ_s is given by the ratio of the transmitted to the incident sound intensity [18] and can be expressed as:

$$\tau_s = \frac{\int_0^L i \cdot \omega \cdot p_t(x,0,\omega) \cdot w_t^*(x,\omega) \cdot dx}{\int_0^L i \cdot \omega \cdot p_i(x,0,\omega) \cdot w_b^*(x,\omega) \cdot dx} \qquad (38)$$

In equation (38), p_t and p_i respectively denote incident and transmitted sound pressures.

The *STL*s for some of the considered core configurations are plotted in Figure 12. As expected, reductions in the *STL* for all the considered configurations occur at the resonance frequencies associated with the modes of transverse vibration. The considered beams become effective as acoustic panels for frequencies higher than their first resonance frequency. In particular, the performance of honeycomb core beams become significantly better than that of square core beams for frequencies above 800 Hz. Among the honeycomb core configurations, reentrant geometries generally provide higher *STL*s than cores with θ>0. The results of Figure 12 hence suggest that selecting negative angles and increasing their value generally improves the sound reduction efficiency of the panel. An explanation of this behavior can be attempted through the observation of the deformed configurations shown in Figures 10 and 11. At higher frequencies, the elements at the core cells resonate and thus undergo high oscillations. Such oscillations are particularly evident for the horizontal elements. Re-entrant geometries have longer horizontal elements, and therefore tend to reach resonance conditions at lower frequencies. In the proposed configuration, each cell may be considered as a

dynamic absorber, whose tuning characteristics depend on the cell geometry. Future studies should carefully examine this behavior and consider the resonance of the cells as a design criterion for increasing the effectiveness of the considered structures as vibration and sound isolators.

The core configuration influences the dynamic behavior of the sandwich beams and modifies their sound radiation pattern. In order to visualize and evaluate the influence of the core on the sound radiation characteristics of the considered beams, the pressure radiated in the acoustic domain is determined through the FT-based procedure presented in this paper. Sound pressure distributions and directivity factors for the considered beams are plotted and compared. The radiated pressure is plotted in the form of Sound Pressure Level (*SPL*), calculated according to the standard formula [19]:

$$SPL(x,y,\omega) = 20\log_{10}\left(\frac{p_t(x,y,\omega)}{p_{ref}}\right) \quad (39)$$

where p_{ref} is the reference pressure, which in air is taken equal to 20 μPa. Using this reference value, the *SPL* corresponding to the amplitude of the incident pressure on the bottom layer, taken equal to 1Pa, is approximately 94 dB.

Examples of Sound Pressure Levels (*SPL*) distributions are shown in Figures 13 through 15, where comparisons between square and honeycomb core with θ=-45° are made for frequency of the incident pressure wave equal to 100, 500 and 1400 Hz. In the maps, the beams are located between x=-0.5 m and x=0.5 m at y=0. The maps show the difference of the distributions of the radiated pressure for the two beams considered for the comparison. At 100 Hz, the amplitude of the pressure radiated by the honeycomb beam is higher than that of the square core, as predicted by the analysis of the *STL* plots shown in Figure 12. The *SPL* radiated by the honeycomb core beam is significantly lower than that of the square core beam at 500 and 1400 Hz (see Figures 14 and 15). A difference can be particularly noticed in Figure 15, which compares the *STL* distributions for the two core configurations for an excitation at 1400 Hz. At this frequency, the radiation of the box-like core is asymmetric with respect to the mid-span line of the beam (x=0), as opposed to all the other distributions presented. Such asymmetric behavior is caused by the influence of the diagonal members of the core on the top-layer deformed configuration at this frequency and on the resulting sound radiation patterns. The directional characteristics of the radiated pressure at the considered excitation frequencies are shown in Figure 16, where the asymmetric behavior of the square core beam at 1400 Hz can be clearly observed.

CONCLUSIONS

This paper analyzes the vibration and acoustic performance of sandwich beams with honeycomb core. The honeycomb geometry is arranged through the thickness as opposed to conventional sandwich honeycomb constructions. The proposed configuration represents an alternative to previously proposed truss core and prismatic material designs. In particular, focus is placed in evaluating the influence of the core geometry and shape on the dynamic structural response and on the sound radiation of the considered class of beams. A comparison is carried out between hexagonal and re-entrant honeycomb configurations, with a square truss core used as baseline.

A finite element is developed to predict the dynamic response of the sandwich beam. The formulation uses dynamic shape functions, which allow for accurate predictions of the structure's dynamic behavior with a reduced number of elements and within a wide frequency range. The formulation is also coupled with a FT-based analysis of the sound radiation in a semi-infinite acoustic domain interacting with one side of the structure. An efficient numerical technique for the prediction of the structural-acoustic behavior of the considered class of beams is thus obtained.

The performance of beams with various core configurations is evaluated and compared in terms of structural response and sound radiation characteristics. The structural analysis shows that beams with honeycomb truss core, particularly with re-entrant geometries, are very effective in reducing the transmission of vibrations through the core. The vibration reduction mechanism is related to the deformation of the core members, which can be properly designed to achieve optimum performance within a specified frequency range. The honeycomb truss core beams also show superior sound transmission reduction capabilities. The improvement in sound reduction is particularly evident at high frequencies and for cores with re-entrant geometry.

The results presented in this paper show the potential advantages of a truss core with honeycomb topology and indicate that re-entrant configurations are generally more effective for vibration and sound transmission reduction applications. The presented results focus only on the assessment of the influence of the core internal angle, for a fixed number of cells along the length of the beam and across its thickness. Further studies should investigate the effect of the cell dimensions and assess the performance of other alternative layouts. The analysis should be then extended to plates with three-dimensional truss cores. Finally, the developed numerical model should be validated experimentally.

ACKNOWLEDGMENTS

The author wishes to thank the National Science Foundation for the support provided for this work under the grant CMS-0201371.

REFERENCES

[1] **Gibson, L.J., Ashby, M. F.,** *Cellular solids: Structure and Properties*, 2nd Edition, 1997, Cambridge University Press, Cambridge, UK.

[2] **Evans, A.G., Hutchinson, J.W., Fleck, N.A., Ashby, M.F., Wadley, H.N.G.,** "The Topological Design of Multifunctional Cellular Metals", *Progress in Materials Science* 46 (2001), 309-327.

[3] **Ashby M.F., Evans A.G., Fleck N.A., Gibson L.J., Hutchinson J.W., Wadley H.N.G.** *Metal Foams: a Design Guide,* Butterworth-Heinemann, June 2000.

[4] **Wallach, J.C., Gibson, L.J.** "Mechanical behavior of a three-dimensional truss material" *International Journal of Solids and Structures* 38 (2001), 7181-7196.

[5] **Wicks, N., Hutchinson, J.W.**, "Optimal Truss Plates" *International Journal of Solids and Structures* 38 (2001), 5165-5183.

[6] **El-Raheb**, **M.**, "Frequency response of a two-dimensional trusslike periodic panel" *Journal of the Acoustical Society of America* **101**(6), June 1997, 3457-3465.

[7] **El-Raheb, M., Wagner, P.** "Transmission of sound across a trusslike periodic panel: 2D analysis" *Journal of the Acoustical Society of America* **102**(4), October 1997, 2176-2183.

[8] **Scarpa, F. and Tomlinson, G.**, "Theoretical characteristics of the vibration of sandwich plates with in-plane negative Poisson's ratio values" *Journal of Sound and Vibrations* **230**(1), 2000, pp. 45-67.

[9] **Herakovich, C. T.**, "Composite laminates with negative through-the-thickness Poisson's ratios". *J. Comp. Mat*. **18**, 1984, pp. 447-455.

[10] **Evans, K. E.**, "Design of doubly curved sandwich panels with honeycomb cores". *Comput. Structs*, **17**(2), 1991, 95-111.

[11] **Ruzzene, M., Soranna F., Scarpa F., "**Wave Beaming Effects In Bi-Dimensional Cellular Structures" Accepted for publication *Smart Materials and Structure,* 2003.

[12] **Doyle, J.F.**, *Wave Propagation in Structures* 2nd Edition, 1997, Springer Verlag, New York, NY.

[13] **Doyle, J.F.**, "A spectrally-formulated Finite Element for longitudinal wave propagation." *Int. Journal of Analytical and Experimental Modal Analysis,* 3 (1988), 1-5.

[14] **Gopalakrishnan S., Doyle J.F.**, "Wave propagation in connected wave guides of varying cross section", *Journal of Sound and Vibration*, **175**(3), 1994, 347-363.

[15] **Petyt, M.**, *Introduction to Finite Element Vibration Analysis,* 1990, Cambridge University Press, New York, NY.

[16] **Love, A.E.H.**, *A Treatise on the Mathematical Theory of Elasticity,* 4th Edition, Dover Publications, New York, NY.

[17] **Junger, M.C., Feit, D.,** *Sound, Structures and Their Interaction,* 2nd Edition, The Acoustical Society of America 1993.

[18] **Fahy, F.,** *Sound and Structural Vibration: Radiation, Transmission and Response,* Academic Press, 1985.

[19] **Kinsler, L.E., Frey, A.R., Coppens, A.B., Sanders, J.V.,** *Fundamentals of Acoustics,* 4th Edition, 2000 John Wiley and Sons, New York, NY.

FIGURES

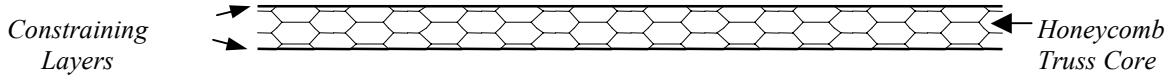

Figure 1: Schematic of beam with honeycomb truss core.

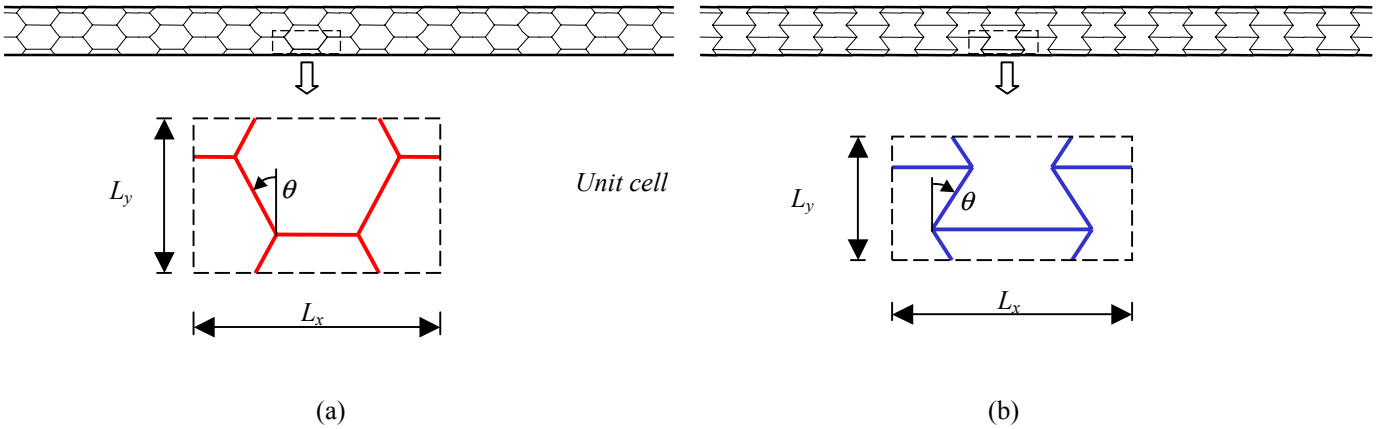

Figure 2: Dimensions and geometry of the core unit cell: hexagonal honeycomb core (a), re-entrant honeycomb core (b).

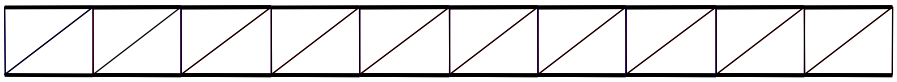

Figure 3: Truss core beam with "square" core.

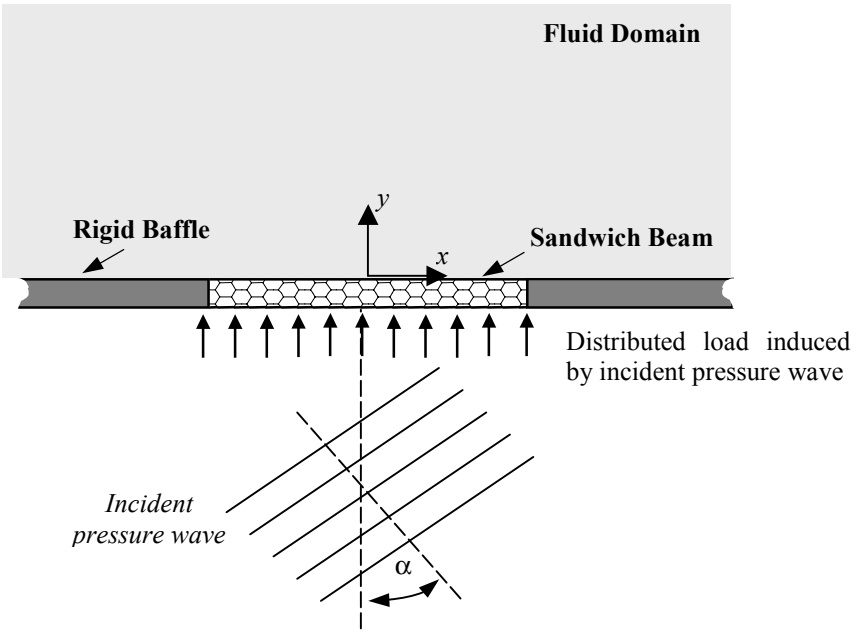

Figure 4: Considered loading and radiation condition for the baffled sandwich beam.

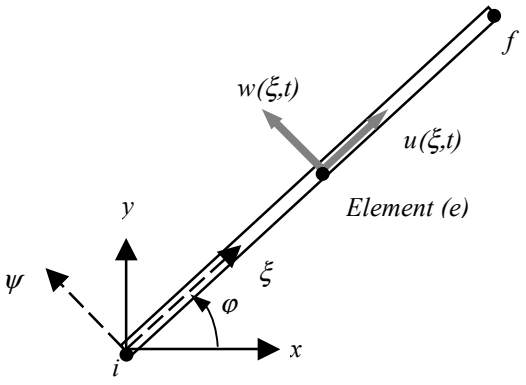

Figure 5: Global and local reference systems and element degrees of freedom.

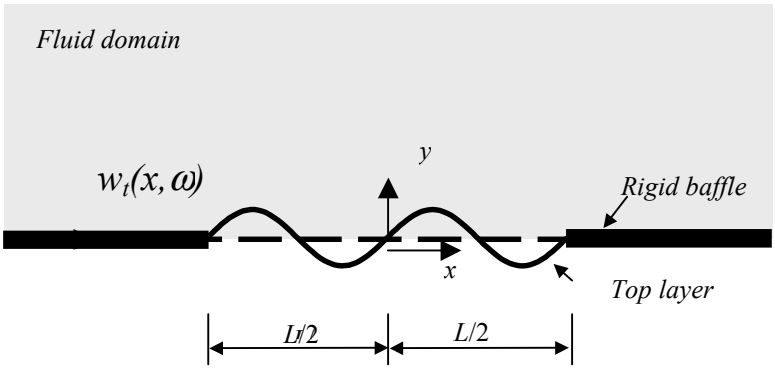

Figure 6: Schematic representation of top layer-fluid interface.

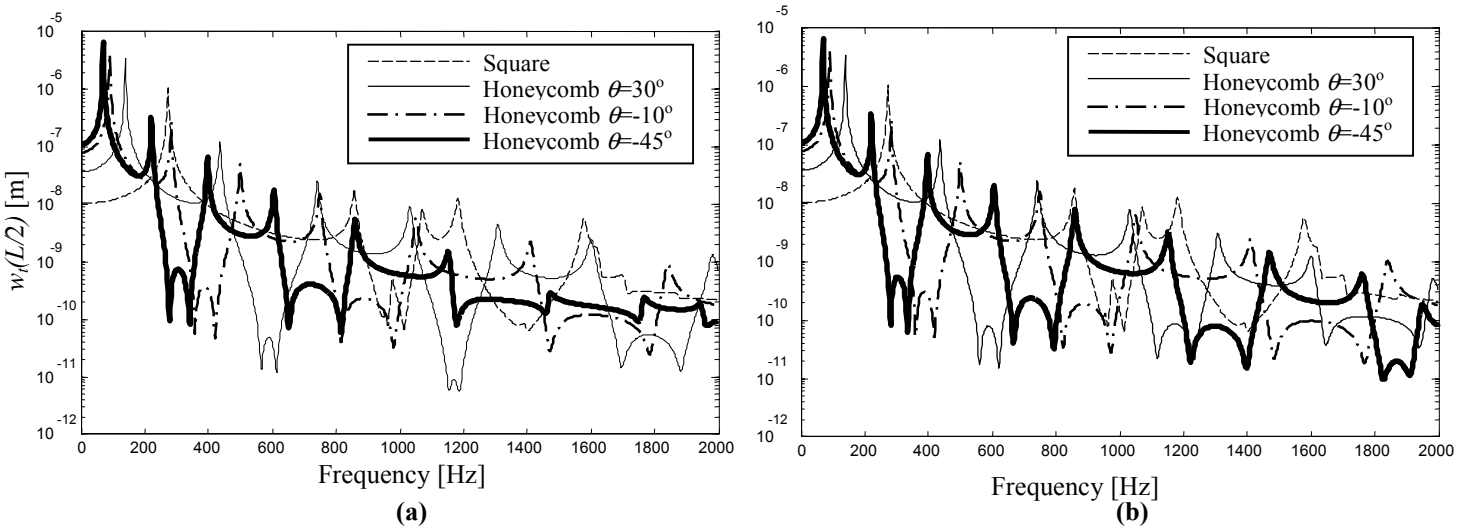

Figure 7: Displacements at mid-span of top (a) and bottom (b) layer for normally incident plane pressure on bottom layer.

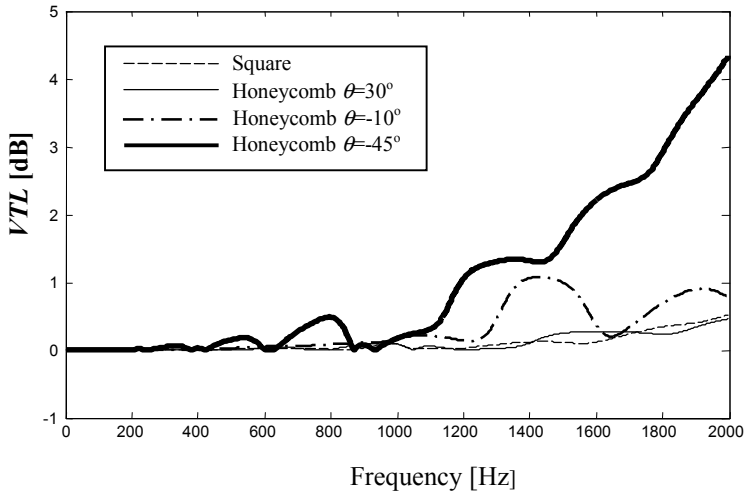

Figure 8: Vibration Transmission Loss (*VTL*) for various core configurations.

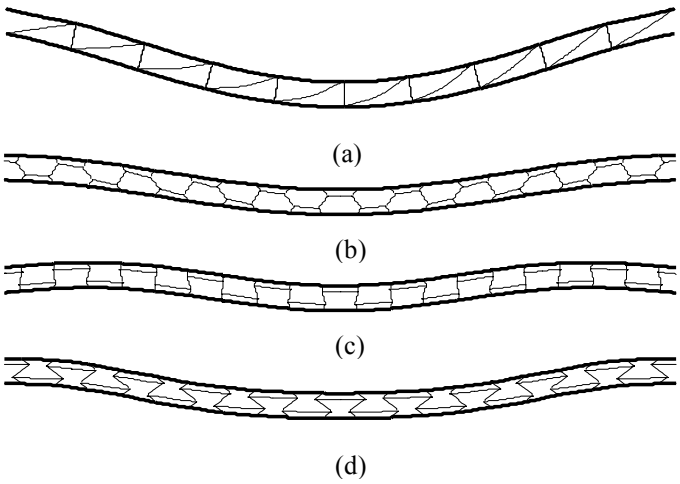

Figure 9: Deformed configurations for excitation at 200 Hz. Square core (a), θ=30° (b), θ=-10° (c) and θ=-45° (d).

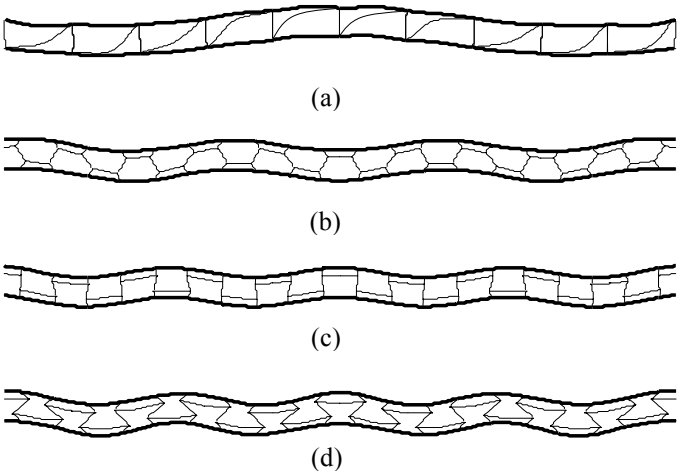

Figure 10: Deformed configuration for excitation at 800 Hz. Square core (a), θ=30° (b), θ=-10° (c) and θ=-45° (d).

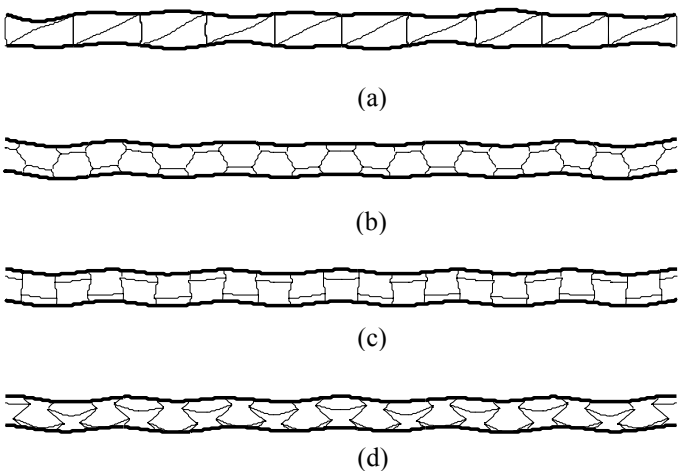

Figure 11: Deformed configuration for excitation at 1500 Hz. Square core (a), θ=30° (b), θ=-10° (c) and θ=-45° (d).

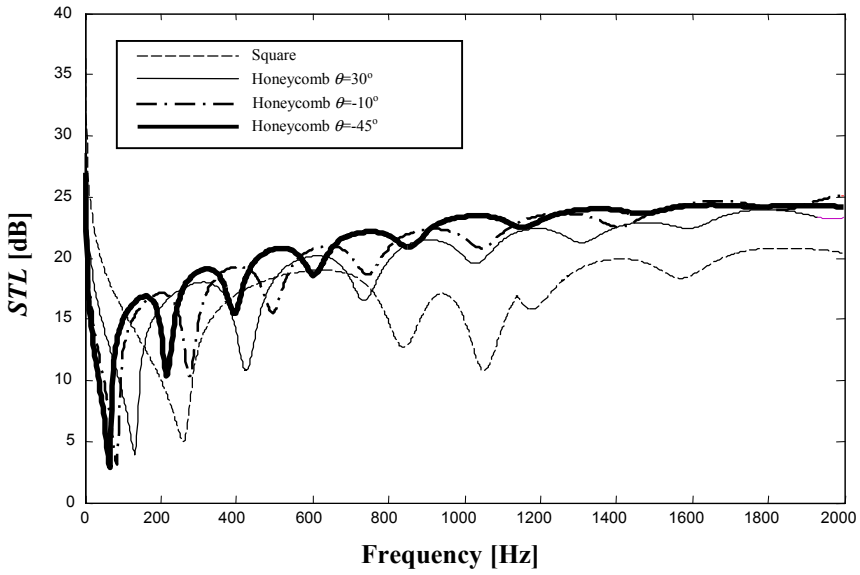

Figure 12: Sound Transmission Loss (*STL*) for various core configurations

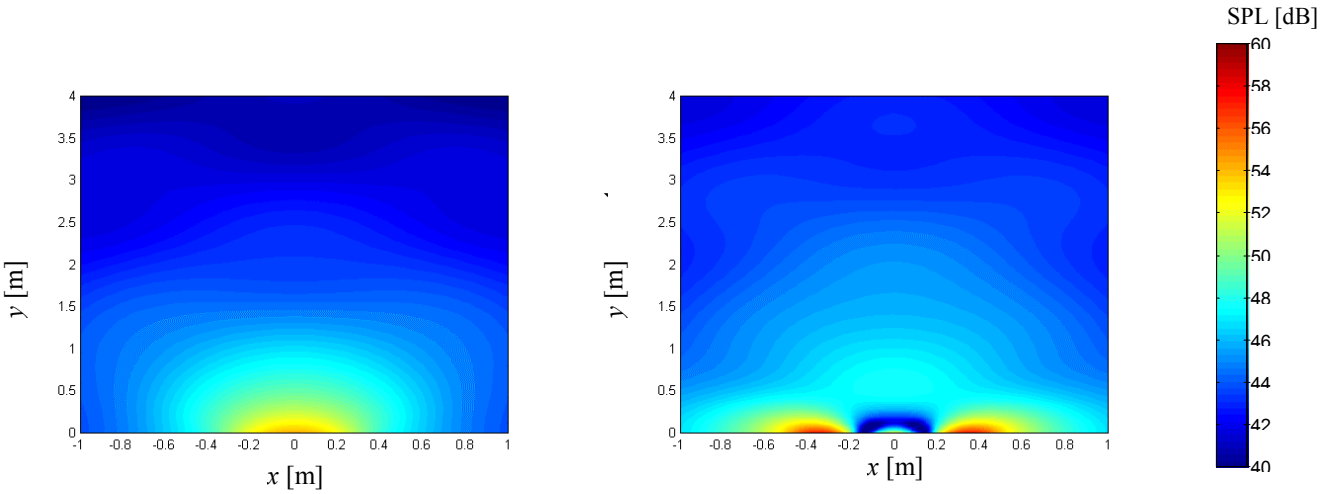

Figure 13: Radiated Sound Pressure Levels at 100 Hz. Square core (a), re-entrant core with θ=-45° (b).

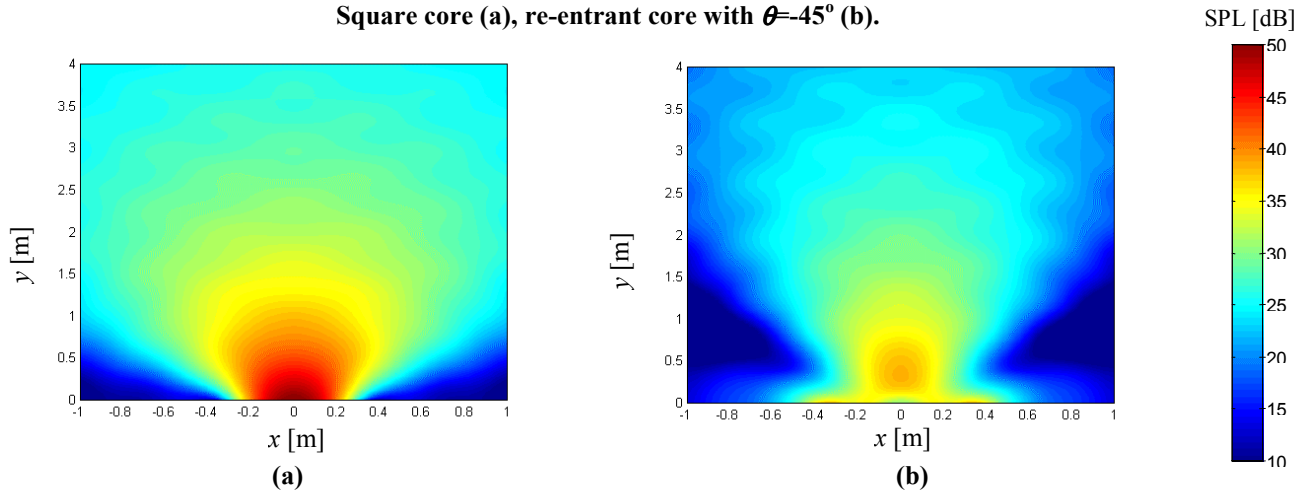

Figure 14: Radiated Sound Pressure Levels at 500 Hz. Square core (a), re-entrant core with θ=-45° (b).

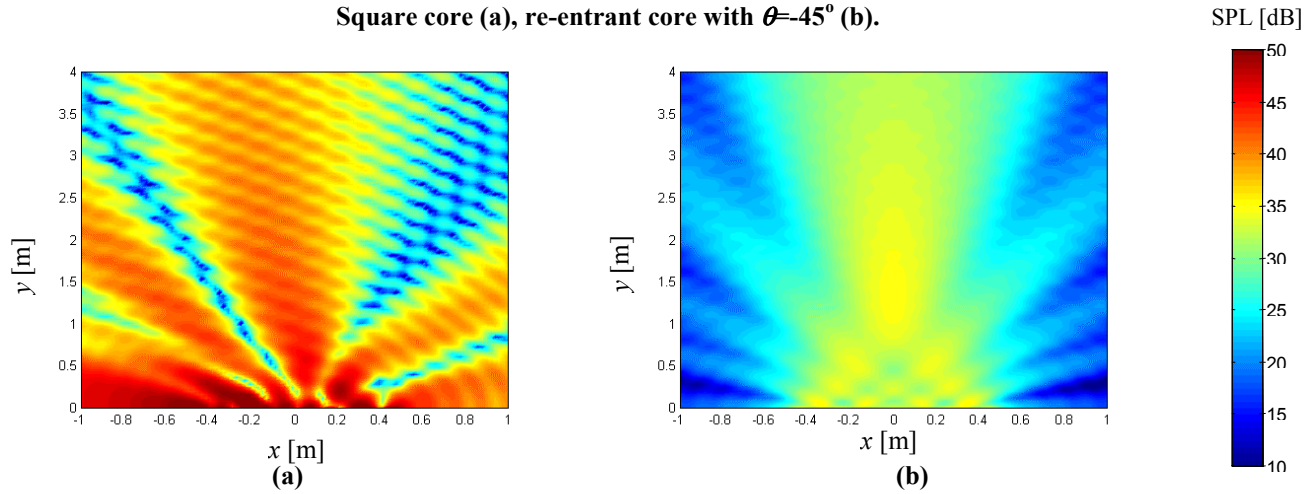

Figure 15: Radiated Sound Pressure Levels at 1400 Hz. Square core (a), re-entrant core with θ=-45° (b).

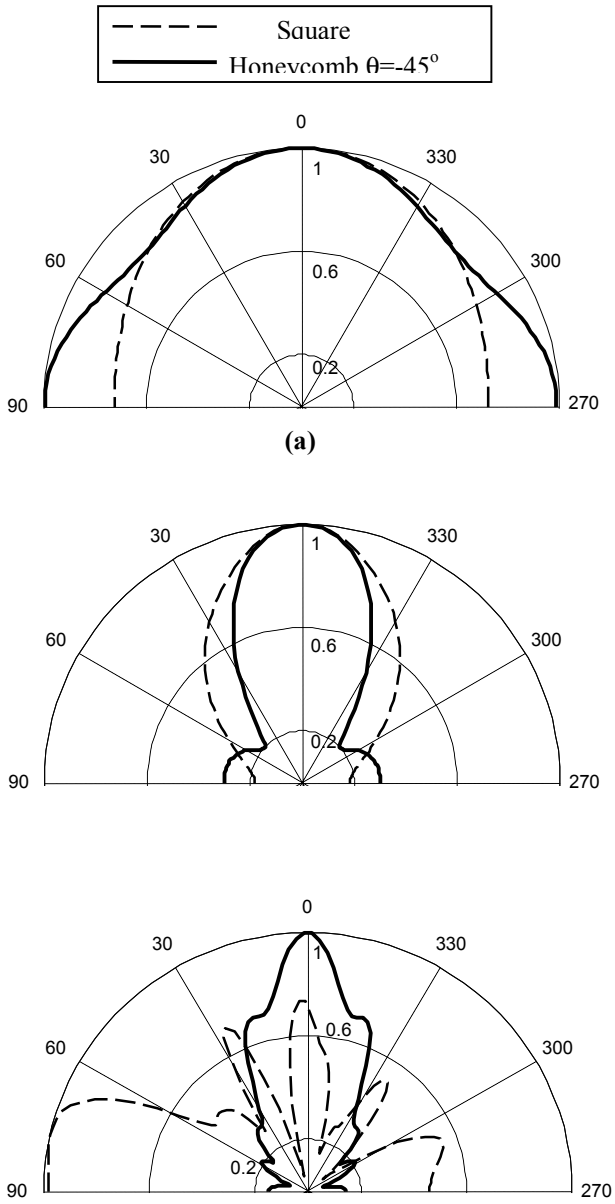

Figure 16: Directivities at 100 Hz (a), 500 Hz (b), and 1400 Hz (c).